Boundary-Layer Meteorol (2007) 123:219–237
DOI 10.1007/s10546-006-9127-8

ORIGINAL PAPER

Effects of mesoscale sea-surface temperature fronts on the marine atmospheric boundary layer

Eric D. Skyllingstad · Dean Vickers · Larry Mahrt · Roger Samelson

Received: 2 December 2005 / Accepted: 29 August 2006 / Published online: 19 October 2006

Abstract A numerical modelling study is presented focusing on the effects of mesoscale sea-surface temperature (SST) variability on surface fluxes and the marine atmospheric boundary-layer structure. A basic scenario is examined having two regions of SST anomaly with alternating warm/cold or cold/warm water regions. Conditions upstream from the anomaly region have SST values equal to the ambient atmosphere temperature, creating an upstream neutrally stratified boundary layer. Downstream from the anomaly region the SST is also set to the ambient atmosphere value. When the warm anomaly is upstream from the cold anomaly, the downstream boundary layer exhibits a more complex structure because of convective forcing and mixed layer deepening upstream from the cold anomaly. An internal boundary layer forms over the cold anomaly in this case, generating two distinct layers over the downstream region. When the cold anomaly is upstream from the warm anomaly, mixing over the warm anomaly quickly destroys the shallow cold layer, yielding a more uniform downstream boundary-layer vertical structure compared with the warm-to-cold case. Analysis of the momentum budget indicates that turbulent momentum flux divergence dominates the velocity field tendency, with pressure forcing accounting for only about 20% of the changes in momentum. Parameterization of surface fluxes and boundary-layer structure at these scales would be very difficult because of their dependence on subgrid-scale SST spatial order. Simulations of similar flow over smaller scale fronts (<5 km) suggest that small-scale SST variability might be parameterized in mesoscale models by relating the effective heat flux to the strength of the SST variance.

Keywords Internal boundary layer · Large-eddy simulation · Marine boundary layer · SST variability

E. D. Skyllingstad (✉) · D. Vickers · L. Mahrt · R. Samelson
College of Oceanic and Atmospheric Sciences, Oregon State University, 104 COAS Admin Bldg, Corvallis, OR 97331-5503, USA
e-mail: skylling@coas.oregonstate.edu

1 Introduction

A basic understanding of coupling between the ocean and atmosphere is necessary for accurate prediction of the atmosphere/ocean circulation at nearly all scales. For example, seasonal forecasts of the El Nino/Southern Oscillation depend on realistic representation of wind-stress forcing on the equatorial Pacific Ocean. At large scales, satellite scatterometry indicates that wind-stress patterns are closely correlated with sea-surface temperature (SST) throughout the world's ocean (e.g. Liu et al. 2000; Chelton et al. 2001, 2004; O'Neill et al. 2003). Smaller scale coupling has been noted in mid-latitude regions, for example, near the Gulf Stream off the coast of North Carolina (Mahrt et al. 2004). In that study, aircraft data show that for flow from warm to cold water, the winds close to the surface decelerate over the cold water and may decouple from the large-scale flow aloft, forming a separate, internal boundary layer (IBL). Similar decoupling events have been reported in Smedman et al. (1997) and Mahrt et al. (2001), with the IBL persisting for hundreds of km downwind from the SST transition.

Historically, research focusing on wind/SST coupling has centered on tropical regions, where measurements first indicated a significant connection between winds and SST. Two main hypotheses have been presented explaining why the wind field changes for flow over SST variations. Lindzen and Nigam (1987) proposed that most of the variation in the winds is caused by a pressure effect, whereby warming of the atmosphere over high SST regions causes a reduction in pressure via the hydrostatic balance, with a commensurate increase in pressure over cooler water. Because changes in the surface heat flux take time to affect the atmospheric temperature, the pressure effect proposed by Lindzen and Nigam requires scales of motion on the order of hundreds of kilometres, depending on the atmospheric stability and wind speed. An alternative to the pressure hypothesis presented in Wallace et al. (1989) contends that vertical momentum transport by turbulence could account for changes in the surface winds. In their theory, convective mixing of momentum over warmer water causes an increase in near-surface winds by transporting faster moving air downward to the surface. More recently, Samelson et al. (2006) explored the idea of the vertical momentum budget control by using a simple two-layer model. They found that changing the depth of the stress boundary layer and therefore stress divergence could explain the changes in wind speed produced by SST variations, following Wallace et al. (1989).

Much of the effort in understanding how SST variations affect wind speed has centered on the offshore flow of cold air over warm water and the formation of an IBL (e.g. Attie and Durand 2003). In these cases, the boundary layer changes in response to both an abrupt increase in surface temperature and a decrease in surface roughness. Less is known about open-ocean scenarios where changes in surface temperature and roughness are smaller. In particular, cases with flow from warm to cold water have only recently been studied using direct flux measurements (Garratt 1990; Vickers et al. 2001; Mahrt et al. 2004). Overall, results from boundary-layer studies agree qualitatively with large-scale observations taken from satellites, showing a positive correlation between wind stress and the SST anomaly (e.g. O'Neill et al. 2003) .

Recent aircraft observations off the coast of Martha's Vineyard in the U.S.A., as part the of the Coupled Boundary Layer Air/Sea Transfer (CBLAST) experiment, have provided wind and temperature data clearly showing the effects of SST fronts on the marine boundary-layer (MBL) structure (Vickers and Mahrt 2006). We present

two examples here representing flow from cold to warm water and warm to cold water. Profiles from the cold to warm case shown in Fig. 1 demonstrate the rapid response of the MBL as the airmass travels over an SST increase of about 3°C over 14 km horizontal distance. On the cold water side of the SST front, low-level wind speeds are relatively weak with significant vertical shear, increasing from 6 m s^{-1} at 10 m to 11 m s^{-1} at 140 m. The turbulence is weak and confined to a shallow layer below about 40 m height. Vertical velocity variance over the warm water is larger and relatively uniform over the 140 m layer, suggesting that enhanced mixing associated with the buoyancy generation of turbulence has increased the MBL depth. The temperature profile over the cool water is quite stable, with an increase of about 2°C over the profile depth. In contrast, the warm profile is nearly constant up to a height of about 110 m, suggesting that the top of the MBL is above the maximum observation.

Probably the most striking difference between the two sides of the SST front is the changes that are evident in the wind speed and potential temperature. For both momentum and potential temperature, turbulent mixing over the warm water downstream appears to have homogenized the MBL structure with near conservation of the total heat and momentum. Because of sampling problems associated with strong surface heterogeneity and limited aircraft coverage, the aircraft data cannot be used to obtain reliable estimates of the vertical fluxes over the SST frontal region. This lack of data is part of the motivation for the current study where we use a large-eddy simulation (LES) model to gain understanding on how the boundary layer is forced when moving over changes in SST. Figure 1 tends to suggest that mixing is the chief mechanism causing the increase in near-surface winds when moving from cool to warm water, agreeing with the hypothesis put forth by Wallace et al. (1989) and clarified by Samelson et al. (2006). However, without accurate pressure measurements, we cannot quantify the importance of the pressure term in the horizontal momentum equation.

Observations of flow from warm to cold water as shown in Fig. 2 are even more difficult to analyze because of the very shallow nature of the IBL that forms when turbulence is reduced by buoyant destruction over the cooler ocean water. The effects of surface cooling have a significant impact on the turbulence strength as shown by the vertical velocity (Fig. 2). At the same time, wind speeds decrease and temperature fluctuations are greatly reduced as the aircraft enters the stratified boundary layer over the cooler water. Aircraft cannot adequately sample the vertical structure in such a shallow boundary layer. Improvements in our understanding of these very shallow boundary layers will require either in situ towers or other novel observation platforms.

The stable boundary layer also poses a significant hurdle for turbulence modelling. For the very stable boundary layer, LES does not resolve the eddy scales responsible for vertical heat and momentum transport. Nevertheless, we can use LES to examine how the boundary layer adapts to the changing SST for regions of the flow that are not strongly stratified. For example, cases that have weakly stratified but fully turbulent flow can be addressed with LES.

In this paper we use LES to examine the changes that occur in the MBL for the two scenarios shown in Figs. 1 and 2. We employ the open boundary version of the LES model described in Skyllingstad et al. (2005) that allows study of discontinuous surface forcing. Two primary questions are addressed using the model: the first question examines the role of the "mesoscale" horizontal pressure gradient in controlling the momentum budget of the boundary layer. Our goal is to evaluate how important

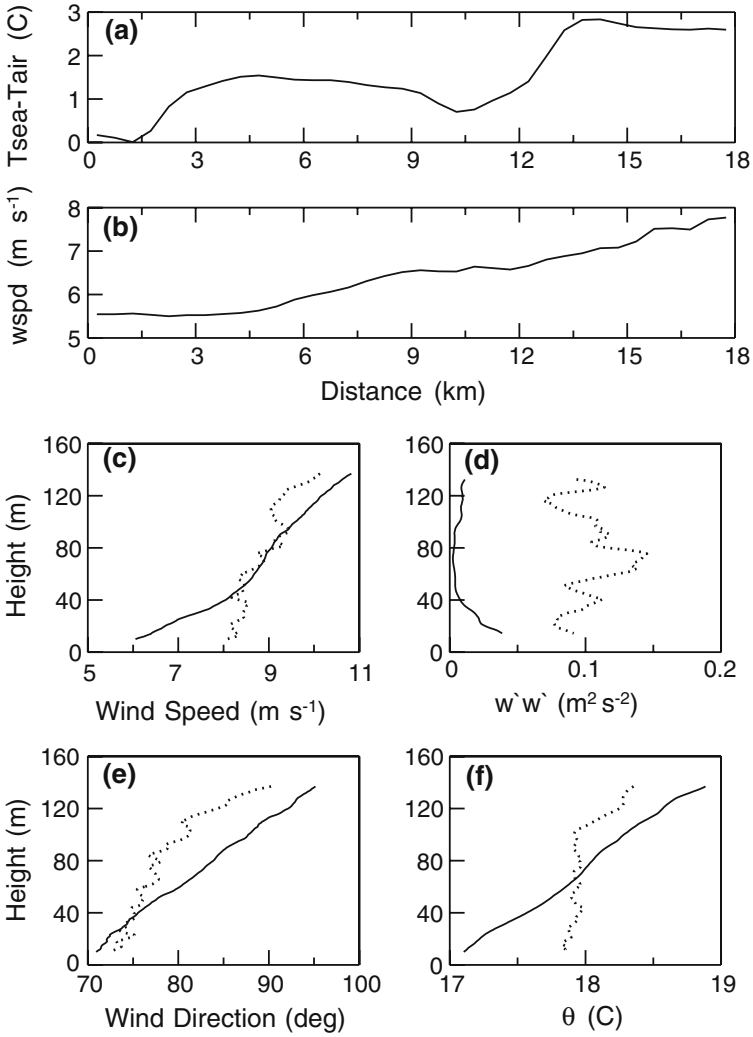

Fig. 1 Aircraft data from early morning on July 30, 2001 showing (**a**) difference between SST and 10-m air temperature, (**b**) and wind speed, (**c**) vertical profiles over cold (solid) and warm (dashed) water of wind speed, (**d**) vertical velocity variance, (**e**) wind direction, and (**f**) potential temperature

this term is in controlling the wind stress versus changes in the vertical mixing rates. The second question focuses on the heat and momentum budgets in regions of changing surface forcing. Most observational and modelling boundary-layer experiments have been applied to approximately homogeneous surfaces. Heterogeneity introduces significant problems in the assessment of heat and momentum budgets by introducing advective terms dependent on mesoscale parameters that are hard to quantify (Nakamura and Mahrt (2005)). Here, we examine how the boundary layer changes in response to a surface front with the goal of identifying whether the order of warming and cooling affects the downstream MBL structure. This issue is of importance when considering the proper resolution for accurate mesoscale simulations.

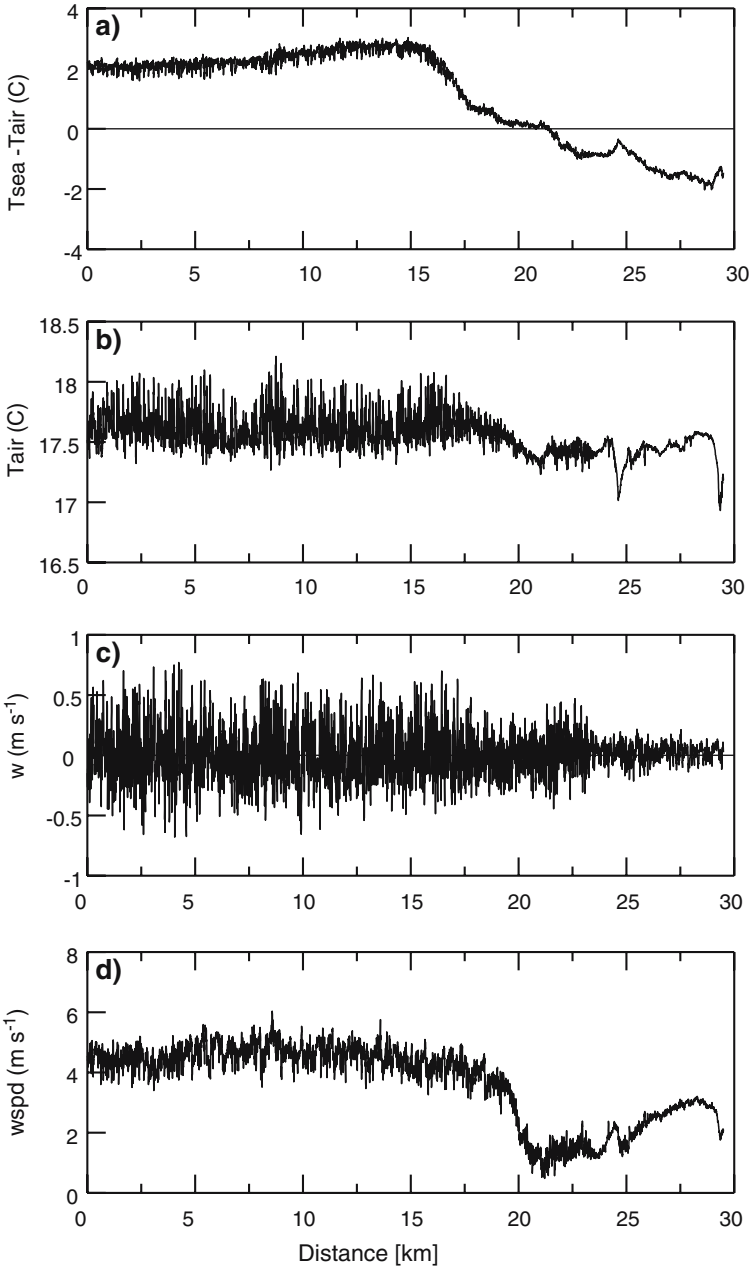

Fig. 2 Aircraft data taken at about 1040 UTC on July 28, 2001 from a height of 10 m showing (**a**) difference between sea-surface temperature and air temperature, (**b**) air potential temperature, (**c**) vertical velocity, and (**d**) wind speed

A brief description of the LES model and methods for initializing the experiments is given in Sect. 2. Section 3 presents an overall picture of the two idealized cases modelled in the study. Heat and momentum budget analysis is presented in Sect. 4, with a summary and conclusions in Sect. 5.

2 Model and initial conditions

Simulations were conducted using the LES model described in Skyllingstad et al. (2005) and Skyllingstad (2003), which is based on the filtered equations described in Deardorff (1980). Subgrid-scale turbulence is parameterized using the filtered structure function model described in Ducros et al. (1996), which sets eddy viscosity according to the strength of resolved turbulent motions. This version of the LES model has been modified to address surface discontinuities by implementing an open outflow condition on the downwind boundary, and a recirculating region with periodic boundary conditions on the upstream boundary following Mayor et al. (2002). Mass conservation is ensured by imposing a vertical velocity on the model top boundary equal to the difference between the average inflow velocity at the edge of the recirculation region, and the average outflow velocity at the downstream boundary. Implementing an upstream recirculation region is equivalent to running a separate LES case for a periodic domain, and then using the flow variables on the model boundary as input conditions for the upstream inflow boundary.

Surface forcing is prescribed using the Louis (1979) scheme with a prescribed lower boundary SST and wind-speed dependent surface roughness length (Fairall et al. 1996). As a simplification, latent heat flux is not considered in the simulations. Initial conditions were prescribed using a uniform profile of potential temperature from the surface to 80 m with potential temperature of 290 K, capped by an inversion with a vertical potential temperature gradient of $0.015\,\mathrm{K\,m^{-1}}$. Winds in the model were initialized in geostrophic balance, with a velocity of $6\,\mathrm{m\,s^{-1}}$.

Simulations were performed using a channel configuration with a domain size of 30.72 km in the along-flow direction, 0.8 km in the cross-flow direction, and 200 m in the vertical direction with a grid spacing of 4 m. Recirculation was performed over a sub-region of 1.28 km (320 grid points) along the left-hand side of the domain. Two cases were examined representing warm to cold (WC) and cold to warm (CW) transitions over an approximately 20 km region in the middle of the model domain. Sea surface temperature was divided into four zones as summarized in Table 1. In zone 1 the SST is set equal to the initial boundary-layer temperature, 290 K, generating a neutral, shear driven boundary layer as the upwind flow for both simulations. Simulated conditions over zone 1 are nearly equivalent for both cases. Variations in SST were prescribed in zones 2 and 3 by setting each region to a constant SST, but alternating between cooling and heating in the two cases examined here. Zone 4 returned the SST to the background value of 290 K before the air mass exited the model domain. Simulations were conducted for 80 min, which was long enough for the boundary-layer structure to reach near steady state.

3 Boundary-layer structure

We first examine the boundary-layer structure for the two cases by presenting cross-sections from the model at the end of the respective simulations in Figs. 3 and 4. In

Table 1 Description of sea-surface temperature forcing and simulations

	Zone 1 $X = 0$–4.48 km	Zone 2 $X = 4.48$–14.08 km	Zone 3 $X = 14.08$–23.68 km	Zone 4 $X = 23.68$–30.72 km
Case WC	290 K	292 K	288 K	290 K
Case CW	290 K	288 K	292 K	290 K

Case WC (Fig. 3), surface heating in zone 2 generates convective mixing that extends from the surface to 150 m where eddies impinge on the background initialized stratification. Overall, the boundary layer over the warm water is relatively well-mixed for heat and momentum. As the air travels over the colder surface (zone 3), the boundary layer divides into two regions. Near the surface, an IBL forms with much cooler air, stronger stratification, and weaker turbulence. This IBL deepens gradually to about 30 m before reaching the end of the cooling region at $x = 23.68$ km. In the remnant layer above the IBL, turbulent eddies transported over the cooler water gradually decay due to dissipation and the expenditure of energy against buoyancy as warmer air above the MBL is entrained downward, and cold air from the new stratified IBL is mixed upward. The IBL persists beyond the cold water region, and begins to mix upward more rapidly in response to relatively warmer water in zone 4. However, stable stratification forced by surface cooling in zone 3 limits vertical mixing so that the two-layer structure persists all the way across zone 4 to the model boundary. The thermally induced pressure gradient in this case is very small over zones 1 and 4, but forms a near constant, weak horizontal gradient as the MBL moves over the warm and cool water zones.

Case CW (Fig. 4) presents a markedly different scenario from Case WC even though the total heat content of the upper ocean represented by the SST changes is essentially the same. In zone 1, the two cases are statistically equivalent as noted above. As the air moves downstream over zone 2, surface cooling quickly generates an IBL that is similar to the cold zone in Case WC, but with much weaker turbulence in the remnant boundary layer above the IBL because there is no intervening zone of surface heating. Even so, the depth of the cold IBL in case CW appears greater in comparison with the cold IBL shown in Fig. 3 with case WC. Subsequent movement of the air over the warm water zone 3 region causes the rapid production of convective eddies, increased vertical mixing, and destruction of the cold IBL.

Horizontally averaged profiles over zone 1 and sub-sections of zones 2 and 3 (Fig. 5) provide a bulk view of the boundary-layer transformation forced by the changing SST. We chose sub-section averages over the warm and cold water zones to emphasize the change in MBL structure. In Case WC, profiles show a typical, neutral MBL in zone 1 with a nearly uniform potential temperature in the vertical. Convective forcing over zone 2 generates strong mixing as shown by the increased vertical velocity variance and well-mixed horizontal velocity and potential temperature. Over zone 3, surface cooling forces a two-layer structure effectively isolating the upper portion of the boundary layer (referred to as a remnant boundary layer) from the surface, with the cool IBL having stronger shear and stratification in comparison with the remnant mixed layer between 40–120 m height. Turbulence, as indicated by the vertical velocity variance, decreases dramatically with downstream distance because of stable stratification and isolation from the remnant boundary layer. Horizontal momentum

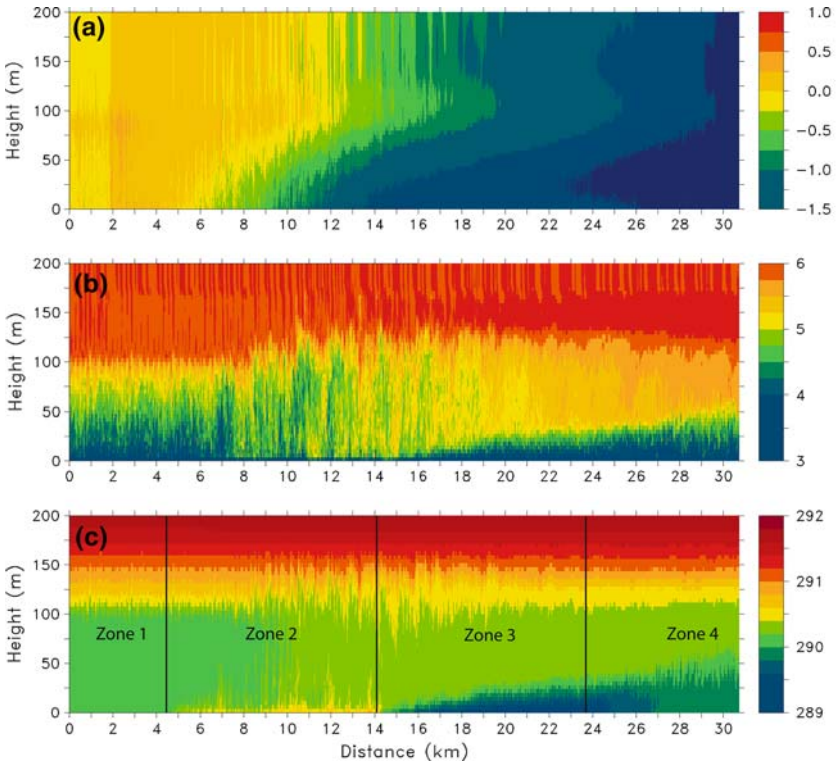

Fig. 3 Cross-sectional plots in the vertical and horizontal direction at $y = 126$ m for Case WC showing (**a**) perturbation pressure (Pa), (**b**) horizontal velocity ($\mathrm{m\,s^{-1}}$), and (**c**) potential temperature (K) after 80 min. Sea surface temperature in this case is 290 K in Zone 1, 292 K in Zone 2, 288 K in Zone 3, and 290 K in Zone 4

in the remnant mixed layer is greater over the cold zone 3 in comparison with the warm zone 2, since decoupling from the surface shear stress leads to flow acceleration. However, most of this change is due to decreasing momentum over zone 1, which has not yet propagated downstream (see budget discussion in the next section).

Vertical profiles over the warm and cold zones for case CW are similar to Case WC with some notable differences. In both cases the vertical velocity variance is a maximum over the warm water, especially in case CW. Warming in case WC generates a greater increase in boundary-layer temperature because of stronger entrainment of air from the overlying stable inversion layer (above 120 m). Entrainment is weaker in case CW because surface forced convection over zone 3 must first erode the cold IBL before entrainment can transport warmer air downward from the upper-level inversion.

Case CW represents a scenario similar in some ways to the observational case presented in Fig. 1, such as the observed wind speed transition from a nearly constant vertical gradient over the cold water to well-mixed conditions over the warm water. Mixing in the simulation produces a similar result, although shear over the cold zone is more intense near the surface because of the well-defined IBL. We do not see the overturning of potential temperature as suggested by the profiles in Fig. 1f. Simulated

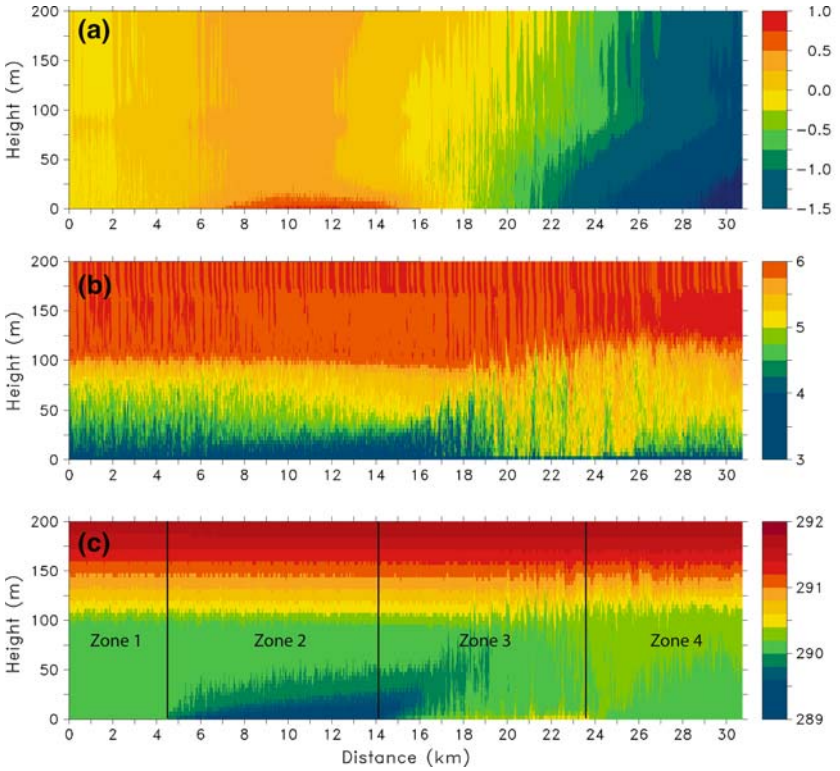

Fig. 4 Same as Fig. 3, except for Case CW. Sea surface temperature in this case is 288 K under Zone 2 and 292 K under Zone 3

potential temperature always shows an increase as the boundary layer travels over the warm zone, whereas the observations indicate a cooling for air above 70 m. Such cooling is only possible if most of the mixing is due to mechanical stirring, which seems unlikely given the convective forcing by the warm water. Alternatively, the atmosphere may have warmed by advection aloft.

A qualitative comparison between Case WC and the flight data presented in Fig. 2 can be made by plotting potential temperature, vertical velocity, and wind speed at 10 m height as shown in Fig. 6. Overall, the model reproduces the gross qualities of the 10-m structure, such as the decrease in wind speed and temperature when travelling from warm to cold water. Turbulence intensity, as measured by the strength of small-scale perturbations, is not duplicated accurately by the model. For example, aircraft data indicate a significantly smoother data series over the cold water for all of the measured fields, indicating weak turbulence. In comparison, modelled velocity perturbations only decrease slightly and potential temperature variations tend to increase when going from warm to cold water.

What we are probably seeing in the simulation is a limitation of the LES model when trying to simulate stratified turbulence. In the observations, turbulence at the aircraft flight level decreases rapidly in response to increased stratification. Turbulence is less likely to collapse in the numerical model because of the relatively coarse grid spacing and restricted subgrid parameterization, which cannot adequately accommodate

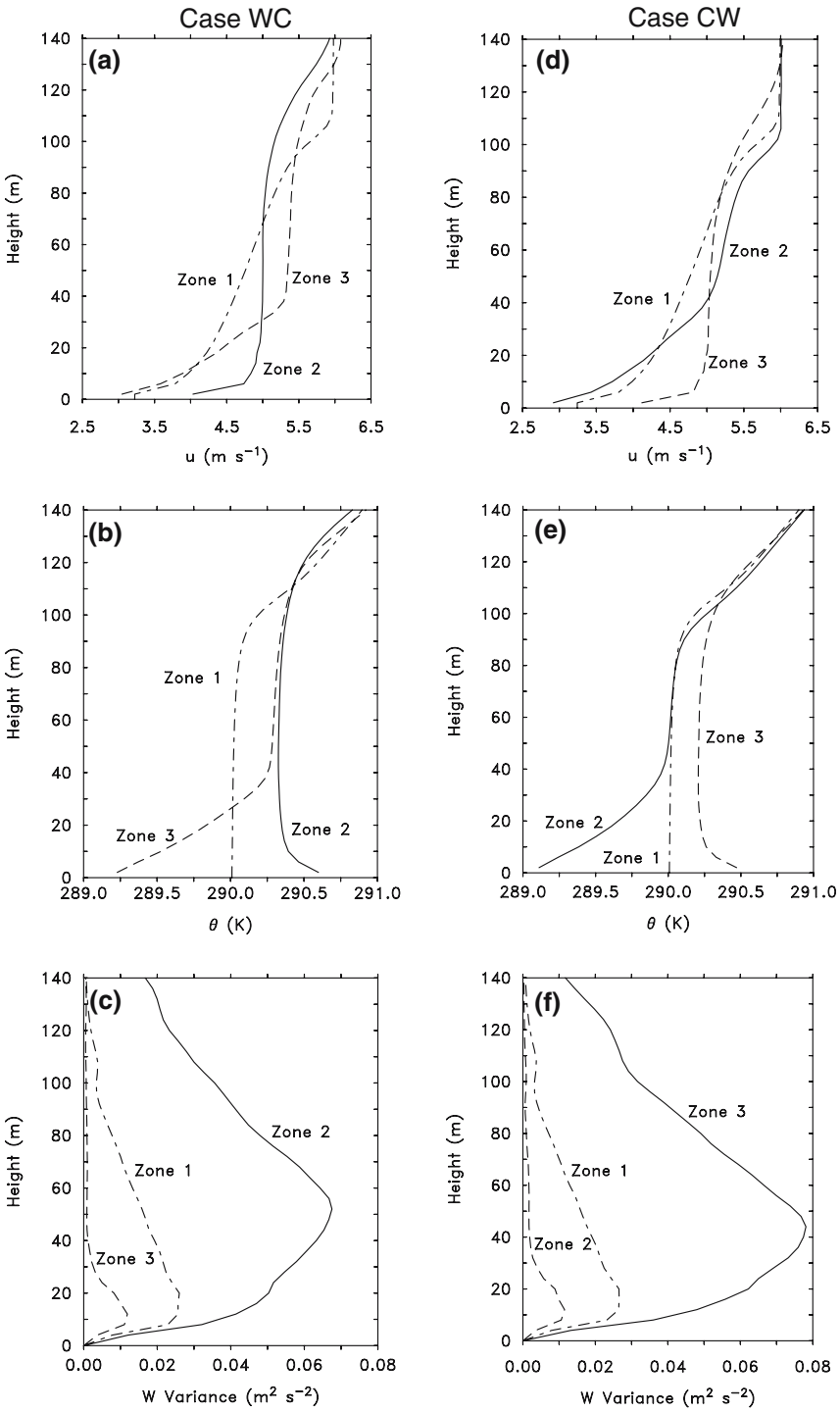
Case WC
Case CW
(a)
(b)
(c)
(d)
(e)
(f)
Height (m)
u (m s^{-1})
θ (K)
W Variance (m^2 s^{-2})
Zone 1
Zone 2
Zone 3

◀ **Fig. 5** Vertical profiles of horizontally averaged (**a**) horizontal velocity, (**b**) potential temperature, and (**c**) vertical velocity variance taken from Case WC (left column) and (**d**) horizontal velocity, (**e**) potential temperature, and (**f**) vertical velocity variance taken from Case CW (right column). Averages are performed between $x = 0$ and 4.48 km (labeled zone 1), $x = 13.44 - 14.08$ (zone 2 subsection) and $x = 23.04 - 23.68$ km (zone 3 subsection)

a thin MBL. In addition, the parameterized roughness length may be too large for the wave conditions that existed in the observations. Nevertheless, the LES model generates a stably stratified boundary layer, but probably with too much turbulence and over a deeper column than would be observed. Because the model has a deeper, more turbulent stable boundary layer, we expect cooling rates to be overestimates of actual conditions, but probably not grossly out of range considering that the observed temperatures also decrease over time.

4 Momentum budget

We calculate the cross-stream average momentum budget by averaging terms in the momentum equation for the u component of velocity, and then decomposing into

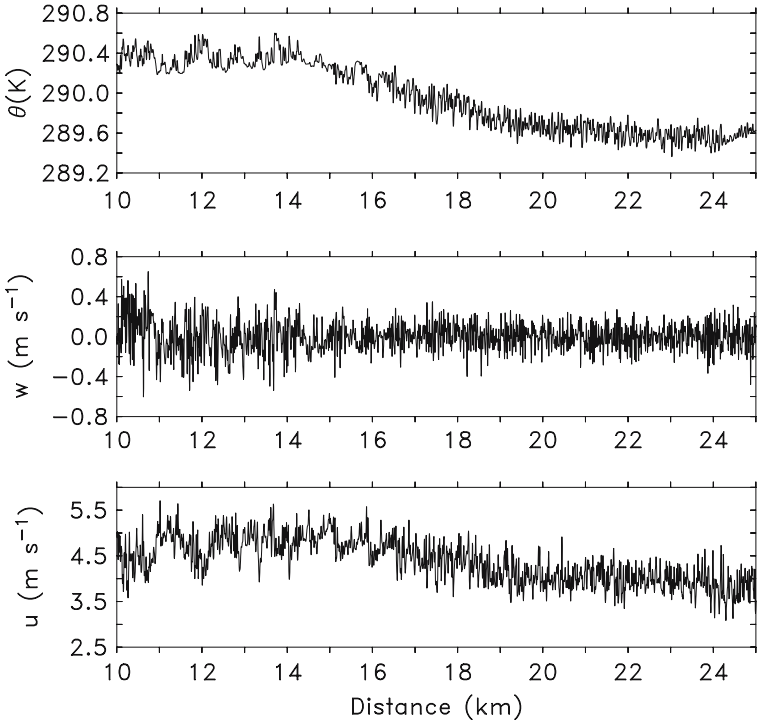

Fig. 6 Simulated values of (**a**) potential temperature, (**b**) vertical velocity, and (**c**) horizontal velocity taken from a height of 10 m at location $y = 126$ m for Case WC. Data overlap the transition region between zones 2 and 3

$u = U + u'$ where $U = \bar{u}$, using the divergence equation and periodic cross-stream boundary conditions, and finally applying averaging rules, obtaining

$$\underset{i}{\frac{\partial U}{\partial t}} + \underset{ii}{U\frac{\partial U}{\partial x}} + \underset{iii}{W\frac{\partial U}{\partial z}} + \underset{iv}{\frac{\partial\left(\overline{u'u'}\right)}{\partial x}} + \underset{v}{\frac{\partial\left(\overline{u'w'}\right)}{\partial z}} = \underset{vi}{-f\overline{V}} - \underset{vii}{\overline{\frac{1}{\rho}\frac{\partial p}{\partial x}}} - \underset{viii}{\frac{\partial\left\langle u''w''\right\rangle}{\partial z}} - \underset{viii}{\frac{\partial\left\langle u''u''\right\rangle}{\partial x}}. \tag{1}$$

Terms in (1) are (*i*) the local tendency or storage term, (*ii*) horizontal advection by the mean wind, (*iii*) vertical advection by the mean vertical motion, (iv) horizontal turbulent flux divergence, (*v*) vertical turbulent flux divergence, (*vi*) Coriolis term, (*vii*) horizontal pressure gradient term, and (*viii*) subgrid-scale mixing term. Double primes in term *viii* indicate subgrid-scale velocities for parameterized fluxes. Terms *v* and *vii* describe the two dominant momentum forcing components discussed in the introduction.

Although observed estimates of the terms in (1) are possible using an array of tower data, calculating horizontal gradients can be very difficult because of surface variations and inadequate instrument coverage. Consequently, momentum budget studies from observations typically look for conditions where term (*v*) is dominant, which can be more easily measured using time-averaged tower data. In the case of ocean aircraft observations, we are limited by much less data. However, if we divide the flow into two regions associated with either the warm or cold water, and then consider the Lagrangian budget for the mean flow between the two regions, we obtain

$$\frac{dU}{dt} = -f\overline{V} - \frac{\partial\left(\overline{u'u'}\right)}{\partial x} - \frac{\partial\left(\overline{u'w'}\right)}{\partial z} - \overline{\frac{1}{\rho}\frac{\partial p}{\partial x}} - \frac{\partial\left\langle u''w''\right\rangle}{\partial z} - \frac{\partial\left\langle u''u''\right\rangle}{\partial x}, \tag{2}$$

where the average advection terms have been combined to form a total derivative or Lagrangian time derivative for the mean flow. Equation 2 indicates that the total change in the mean flow can be attributed to the local turbulent flux terms, Coriolis term and the horizontal mean pressure gradient if we consider how the velocity profile changes between two separate locations, as is shown in Fig. 1.

Analysis of the LES results provides a means of evaluating the momentum budget for transitional flows using (1) and (2). However in analyzing (1), we find that the horizontal and vertical advection terms tend to offset, overwhelming the role of the vertical flux divergence and pressure terms. Because of the large, offsetting terms in the total momentum equation, a more effective way to analyze the model momentum budget is to use the Lagrangian budget described by (2). This is accomplished by first calculating the total change in momentum, $\Delta U/\Delta t$, between the cold and warm water regions using

$$\Delta U/\Delta t = \frac{\frac{1}{N}\left(\sum_{y=23.7\text{ km}}^{24.3\text{ km}} U(z) - \sum_{y=4.5\text{ km}}^{5.1\text{ km}} U(z)\right)}{\Delta t(z)} \tag{3}$$

where sums are also calculated over the cross-stream direction, N is the number of grid points in the two horizontal domain sub-regions and

$$\Delta t(z) = 19200 \sum_{4.8\text{ km}}^{24\text{ km}} \sum_{Sfc}^{200\text{ m}} {}^{1}/_{U(z)} \tag{4}$$

is an estimate of the transit time for a column of air. Equation 3 represents the Lagrangian momentum change when travelling across the SST front. Plots of this term along with the vertical flux divergence and horizontal pressure gradient (averaged over zones 2 and 3) are shown in Fig. 7, and allow us to evaluate the role of turbulence versus pressure forcing.

For both cases, the change in velocity from cold to warm is very similar in form to the vertical momentum flux divergence but with a significant positive offset. As the pressure term shows, the offset is only partially explained by pressure forcing. A much better match between the velocity change and vertical momentum flux is obtained by including the average local change in horizontal momentum, $\partial u/\partial t$, that is produced upstream in zone 1 along with the pressure forcing term, as shown by the right panels in Fig. 7. The Lagrangian description of the flow provided by $\Delta U/\Delta t$ assumes that the upstream flow is near steady state. Then, any changes that occur over the SST front should be local and therefore dominated by the flux divergence and local pressure gradient. However, for a turbulent neutral boundary layer as exists upstream in zone 1, the flow is continually losing momentum to the surface, which is then redistributed vertically throughout the boundary layer. By adding the zone 1 average tendency or storage term to the vertical flux divergence term, we are able to account for the upstream momentum change and obtain a good match between the Lagrangian momentum change and flux divergence.

We note that the pressure term is small in both cases relative to the turbulence flux divergence. This result is in conflict with studies conducted for larger scale flows, for example by Lindzen and Nigam (1987), and indicates that the hypothesis put forth by Wallace et al. (1989) may be more applicable for small-scale SST fronts.

Wind speed profiles shown in Fig. 1 also suggest that convection over the warm water generates a well-mixed boundary layer where the total momentum is basically conserved. This is consistent with the vertical flux divergence having a dominant role in changing the flow field; eddy mixing exchanges momentum vertically, reducing the average shear in the process. However, our simulations suggest that knowing the vertical flux divergence at a single location is not enough to explain how the momentum budget evolves. Measurements over a horizontal range are needed to pin down the important terms in the budget. At a minimum, upstream tendencies are needed so that local effects can be separated from changes that are a direct result of horizontal transport.

Other key factors that determine how the surface wind will respond to changing SST are the strength of the horizontal and vertical transport terms in comparison with the impact of surface drag. If transport terms are small, then changes in the boundary-layer depth should lead directly to changes in the surface wind speed as the surface momentum loss from drag is redistributed over a different boundary-layer depth. For example, a shallow boundary layer will have a slower flow in comparison with a deep boundary layer because of the greater influence of the surface drag term relative to the depth-integrated momentum. Samelson et al. (2006) did a scale analysis of this effect by examining the time scales associated with transport and surface drag, defining a ratio

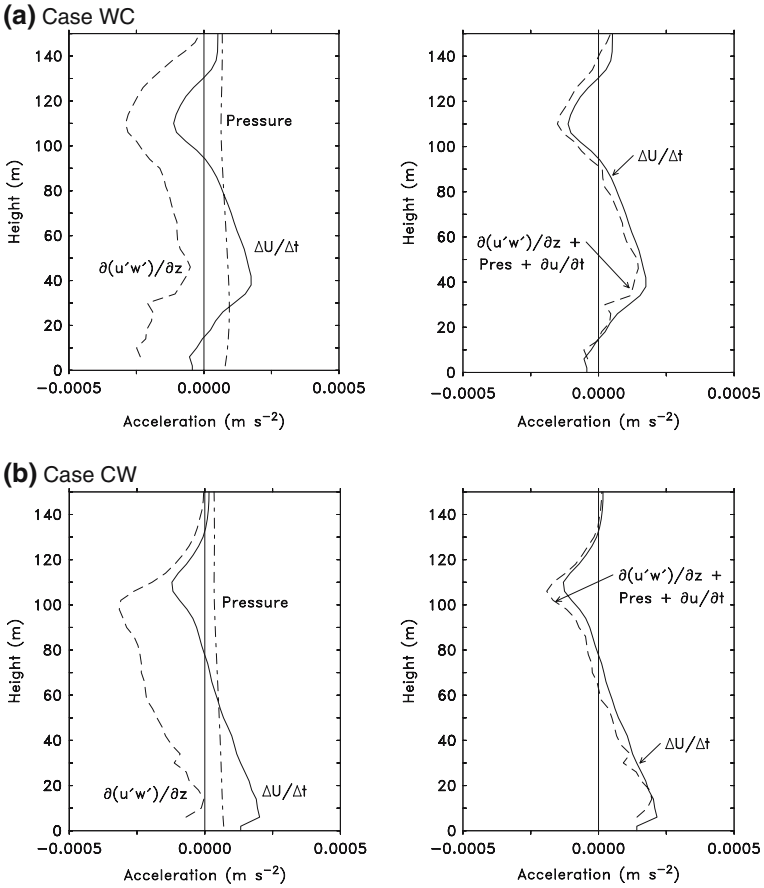

Fig. 7 Horizontal- and time-averaged terms from the momentum budget from Equation (3) for (**a**) Case WC and (**b**) Case CW. Figures on the right side include the upstream momentum tendency and pressure term along with the flux divergence. Terms are defined in the text

$$\gamma_{\tau \mathrm{A}} = \frac{T_\tau}{T_\mathrm{A}} = \frac{hV\Delta V}{\tau L}, \tag{5}$$

where T_τ represents a time scale associated with surface drag, $T_\tau = \frac{h\Delta V}{\tau}$, T_A represents a time scale for horizontal transport effects, $T_\mathrm{A} = \frac{L}{V}$, and h is the boundary-layer depth, V is the average boundary-layer velocity, ΔV is the change in boundary-layer wind speed over the SST transition region, τ is the surface stress and L is a length scale characterizing the SST variations.

When $\gamma_{\tau \mathrm{A}} > 1$, advection dominates over surface friction in controlling horizontal momentum in the boundary layer. Case CW represents an example of this scenario as shown by evaluating $\gamma_{\tau \mathrm{A}}$ over zone 3 using $h = 100$, $V = 4.5\,\mathrm{m\,s^{-1}}$, $\Delta V = 1\,\mathrm{m\,s^{-1}}$, $\tau = 0.03\,\mathrm{N\,m^{-2}}$, and $L = 10\,\mathrm{km}$, yielding $\gamma_{\tau \mathrm{A}} = 1.5$. Heating over the warm region in this case actively forces vertical mixing and downward transport of momentum, increasing the near-surface winds over zone 3. Samelson et al. (2006) identify this mechanism as the *non-equilibrium hypothesis* because the momentum change is controlled by the

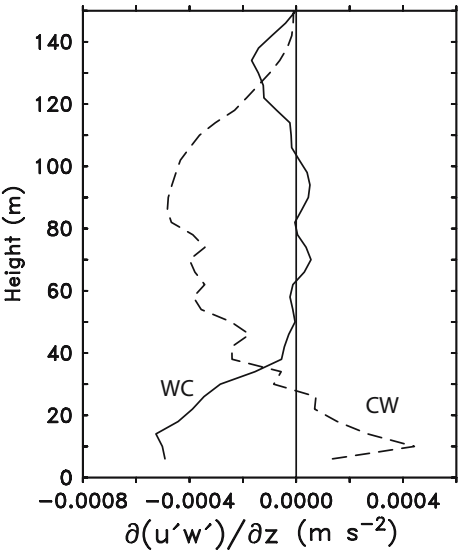

Fig. 8 Horizontal- and time-averaged momentum flux divergence for the horizontal wind component from 80–82 minutes over zone 3

transport of momentum from outside of the boundary layer defined over the cold water region in zone 2.

When $\gamma_{\tau A} < 1$, boundary-layer momentum is controlled primarily by surface wind stress and the depth of the boundary layer as demonstrated in Case WC. Using values over zone 3 of $h = 25\,\mathrm{m}, V = 4.5\,\mathrm{m\,s^{-1}}, \Delta V = 1\,\mathrm{m\,s^{-1}}, \tau = 0.02\,\mathrm{N\,m^{-2}}$, and $L = 10\,\mathrm{km}$, yields $\gamma_{\tau A} = 0.56$. In this case, the warm boundary layer produced over zone 2 decouples when moving over the cold region of zone 3. A shallow boundary layer quickly forms over the cold water, limiting h and decreasing $\gamma_{\tau A}$. Surface wind speed changes in this example are controlled mostly by the surface stress and the shallow boundary-layer depth and the flow is considered to be in *quasi-equilibrium*.

Plots of the vertical momentum flux divergence over zone 3 (Fig. 8) clearly demonstrate how vertical mixing and the mixed-layer depth control the near-surface momentum. In case WC ($\gamma_{\tau A} < 1$), vertical flux divergence is mostly confined to below 40 m where stress is removing momentum from the flow. For this case, changes in the near-surface momentum are generated primarily by surface friction. In contrast, flux divergence for case CW ($\gamma_{\tau A} > 1$) suggests a transfer of momentum from the remnant boundary layer between 35–140 m to the near-surface region.

5 Discussion

Surface flux parameterizations, for example as based on Monin–Obukhov similarity theory, assume that forcing conditions are relatively homogeneous and evolve only slowly in time. Our experiments show that this assumption is not valid when SST varies rapidly over horizontal distances of a few kilometres. To help understand how surface flux variations affect the MBL, we examine the aggregate values for mean temperature and momentum as shown in Fig. 9. These profiles compare the average boundary-layer properties over the region of varying SST (zones 2 and 3), as well as the zone 1 profile predicted upstream from the SST fronts and a profile downstream

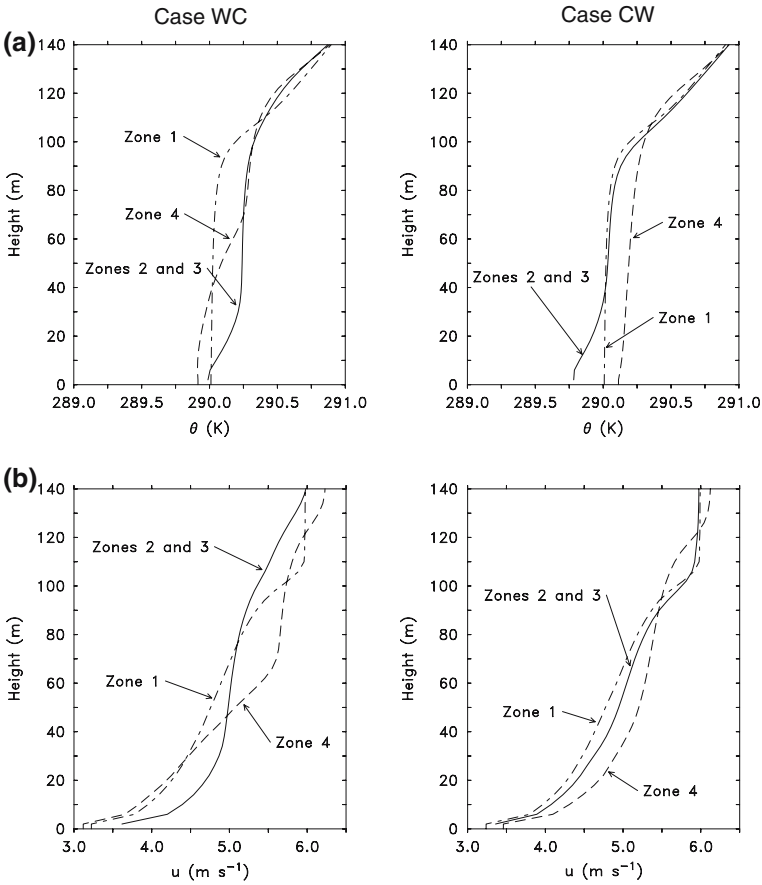

Fig. 9 Vertical profiles of horizontally averaged (**a**) potential temperature and (**b**) horizontal velocity taken from case WC (left) and CW (right) at 80 min from zones representing the frontal transition (zones 2 and 3), upstream conditions (zone 1), and downstream conditions (zone 4)

from the frontal region from zone 4. If we assume that small-scale SST variations are averaged in operational mesoscale models, then the high and low SST used here would tend to offset, resulting in a uniform SST field and a neutral MBL structure similar to the average profile over zone 1.

Comparing the zone 4 profiles between case WC and CW in Fig. 9 indicates that case WC forcing creates the most significant variation in the mean profiles after passing over the frontal zone. As noted above, the potential temperature for zone 2 in case WC is noticeably warmer than the zone 3 average from case CW. Consequently, the mixed layer in case WC is deeper resulting in a greater reduction in wind shear and stronger winds below 80 m over the frontal region. Downstream, the winds decrease near the surface because of the stable boundary-layer that persists after leaving the cold water region. Turbulent fluxes of heat and momentum (not shown) are consistent with the deeper mixed layer, showing more vertical transport and stronger entrainment at the MBL top over the frontal region in case WC. The effects of the cold water in case WC generate a significant negative heat flux between 25–35 m in the zone 4

profile. In comparison, the zone 4 heat flux for case CW is similar to the zone 1 profile with relatively weak values.

As shown by this relatively simple set of experiments, developing a parameterization that accounts for small-scale SST variability poses a big challenge. Our results suggest that subgrid-scale variations in SST can generate significant variations in the boundary-layer structure that are strongly correlated to the degree of surface warming versus cooling and the order in which surface fluxes vary in the downwind direction. When warming is upstream from cooling, the SST variation has a bigger impact because of boundary-layer deepening arising from convective overturning. Cooling upstream from warming generates an internal cold boundary layer that constrains the effects of downstream warming.

Increasing model resolution will reduce this parameterization problem. At what point do SST variations become small enough so that an average value may be used? As a final test, we conducted an experiment with a warm to cold transition reduced in scale so that zone 2 and 3 encompassed just 2.4 km. Average profiles taken from this case over the warm and cold water and just downstream from the frontal region (not shown) suggest that small amplitude SST variations have a minimal effect on the mean properties of the MBL. Nevertheless, the heat flux variations produced by the front (not shown) are still different from the constant SST example.

6 Conclusions

Experiments are presented using a large-eddy simulation model suggesting that relatively small horizontal variations in SST can have a significant impact on the vertical structure of the marine boundary layer over the investigated distances of 10–20 km. Two cases are examined, one for atmospheric flow over an SST transition from relatively cold to warm water, and the second for flow from warm to cold water. Results indicate that mixing is increased in the warm to cold case because of the initial deepening of the boundary layer over the warm water. In the cold to warm case, initial cooling generates a shallow internal boundary layer that initially limits mixing over the warm portion of the domain. The net effect is a deeper boundary layer in the warm to cold case, which causes stronger near-surface winds and greater entrainment of the stable layer at the boundary-layer top.

Surface fluxes are also affected by the history of the flow as the flow passes over the warm and cold water. For example, upward fluxes are larger over the warm water in the cold to warm case because the upstream cooling generates a greater SST gradient over the warm water. Similar effects are noted in the wind stress, but with smaller differences between the two SST scenarios.

Analysis of the momentum budget for both scenarios shows that the most significant term affecting horizontal momentum over the frontal zone is the turbulent vertical flux divergence. Although the thermally forced pressure forcing is significant, it only averages about 20% of the flux divergence term, indicating that for fronts on 10–20 km scales with light winds ($6\,\mathrm{m\,s^{-1}}$) most of the momentum response is produced by turbulent mixing and changes in the boundary-layer depth rather than hydrostatic pressure. Our results agree with scaling arguments presented in Samelson et al. (2006) indicating that the boundary-layer depth controls the downstream strength of near-surface winds in warm to cold transitions, whereas advection and vertical transport are more dominant in cold to warm scenarios.

Boundary-layer changes produced by SST fronts are uniquely defined by the order of the surface forcing (cold to warm versus warm to cold) and would be even more complicated by random SST variations. We therefore hypothesize that accurate parameterization is not feasible for SST variability on larger scales. For smaller scales, a single test using the model over a 2.4 km frontal region suggests that small amplitude variations may have negligible impact on the overall boundary-layer structure. Nevertheless, they do affect the net surface flux, which may be significant in regions with large SST variance. Many of the effects of small-scale SST variability may be already built into flux parameterizations, which are based on large empirical datasets and use average correlations of flux and ΔT data (e.g. Vickers and Mahrt 2006).

Some caution is necessary in considering the conclusions of this study, particularly with regard to the behaviour of the stable boundary layer produced by the downward heat flux over cold water. Although LES produces a cold boundary layer with acceptable average properties, it is likely that the strength of turbulence and resulting fluxes are overestimated for flow over cold water. Further comparisons with observations are needed to verify if the results presented here are representative of actual internal boundary layers produced by surface cooling.

Acknowledgements We would like to acknowledge the supercomputer time provided by the National Center for Atmospheric Research, which is funded by the National Science Foundation. This research was supported by the Office of Naval Research, Grant N00014-01-1-0138 and N00014-05-1-0032, Code 322 MM as part of the CBLAST-low wind project. Support was also provided by the National Science Foundation Grant OCE-0424516.

References

Attie JL, Durand P (2003) Conditional wavelet technique applied to aircraft data measured in the thermal internal boundary layer during sea-breeze events. Boundary-Layer Meteorol 106:359–382

Chelton DB, Esbersen SK, Schlax MG, Thum N, Freilich MH, Wentz FJ, Gentemann CL, McPhaden MJ, Schopf PS (2001) Observations of coupling between surface wind stress and sea surface temperature in the eastern tropical Pacific. J Climate 14:1479–1498

Chelton DB, Schlax MG, Freilich MH, Milliff RF (2004) Satellite measurements reveal persistent small-scale features in ocean winds. Science 303:978–983

Deardorff JW (1980) Stratocumulus-capped mixed layers derived from a three-dimensional model. Boundary-Layer Meteorol 18:495–527

Ducros F, Comte P, Lesieur M (1996) Large-eddy simulation of transition to turbulence in a boundary layer developing spatially over a flat plate. J Fluid Mech 326:1–36

Fairall CW, Bradley EF, Rogers DP, Edson JB, Young GS (1996) Bulk parameterization of air-sea fluxes for tropical ocean-global atmospheric coupled-ocean atmosphere response experiment. J Geophys Res 101:3747–3764

Garratt JR (1990) The internal boundary layer–a review. Boundary-Layer Meteorol 50:171–203

Lindzen R, Nigam S (1987) On the role of sea surface temperature gradients in forcing low-level winds and convergence in the Tropics. J Atmos Sci 44:2418–2436

Liu WT, Xie X, Polito P, Xie S-P, Hashizume H (2000) Atmospheric manifestation of tropical instability waves observed by QuikSCAT and Tropical Rain Measuring Mission. Geophys Res Lett 27:2545–2548

Louis J-F (1979) A parametric model of vertical eddy fluxes in the atmosphere. Boundary-Layer Meteorol 17:187–202

Mahrt L, Vickers D, Sun J, Crawford T, Crescenti G, Frederickson P (2001) Surface stress in offshore flow and quasi-frictional decoupling. J Geophys Res 106:20, 629–20, 639

Mahrt L, Vickers D, Moore E (2004) Flow adjustments across sea-surface temperature changes. Boundary-Layer Meteorol 111:553–564

Mayor SD, Spalart PR, Tripoli GJ (2002) Application of a perturbation recycling method in the large-eddy simulation of a mesoscale convective internal boundary layer. J Atmos Sci 59:2385–2395
Nakamura R, Mahrt L (2005) A study of intermittent nocturnal turbulence with CASES-99 tower measurements. Boundary-Layer Meteorol 114:367–387
O'Neill L, Chelton D, Esbensen S (2003) Observations of SST-induced perturbations of the wind stress field over the Southern Ocean on seasonal timescales. J Climate 16:2340–2354
Samelson RM, Skyllingstad ED, Chelton DB, Esbensen SK, O'Neill LW, Thum N (2006) A note on the coupling of wind stress and sea surface temperature. J Climate 19:1557–1566
Skyllingstad ED (2003) Large-eddy simulation of katabatic flows. Boundary-Layer Meteorol 106:217–243
Skyllingstad E, Samelson R, Mahrt L, Barbour P (2005) A numerical modeling study of warm offshore flow over cool water. Mon Wea Rev 133:345–361
Smedman A-S, Bergström H, Grisogano B (1997) Evolution of stable internal boundary layers over a cold sea. J Geophys Res 102:1091–1099
Vickers D, Mahrt L, Sun J, Crawfordn T (2001) Structure of offshore flow. Mon Wea Rev 129:1251–1258
Vickers D, Mahrt L (2006) Evaluation of air-sea flux bulk formula and sea-surface temperature variability based on aircraft and tower observations. J Geophys Res 111, DOI:10.1029/2005JC003323
Wallace J, Mitchell T, Deser C (1989) The influence of sea-surface temperature on surface wind in the eastern equatorial Pacific: seasonal and interannual variability. J Climate 2:1492–1499